Supplementary Information

Continuous increase in evaporative demand shortened the growing season of European ecosystems in the last decade

Supplementary Information for

Continuous increase in evaporative demand shortened the growing season of European ecosystems in the last decade

Mehdi Rahmati[1,2*], Alexander Graf[2], Christian Poppe[2], Wulf Amelung[3], Wouter Dorigo[4], Harrie-Jan Hendricks Franssen[2], Carsten Montzka[2], Dani Or[5, 6], Matthias Sprenger[7], Jan Vanderborght[2], Niko E. C. Verhoest[8], Harry Vereecken[2]

[1]Department of Soil Science and Engineering, University of Maragheh, Maragheh, Iran

[2]Agrosphere Institute IBG-3, Forschungszentrum Jülich GmbH, 52425 Jülich, Germany

[3]Institute of Crop Science and Resource Conservation (INRES)- Soil Science and Soil Ecology, University of Bonn, Bonn, Germany

[4] Department of Geodesy and Geoinformation, TU Vien, Vienna, Austria

[5]Department of Environmental Systems Science, ETH Zurich, Switzerland

[6]Division of Hydrologic Sciences (DHS) - Desert Research Institute, Reno, NV, USA

[7]Lawrence Berkeley National Laboratory, Berkeley, California, USA

[8]Hydro-Climate Extremes Lab, Ghent University, Ghent, Belgium

*Corresponding authors: Mehdi Rahmati: mehdirmti@gmail.com, m.rahmati@fz-juelich.de

The PDF file includes supplementary Figures 1–12, supplementary Table 1, supplementary note, and supplementary discussions 1 and 2.

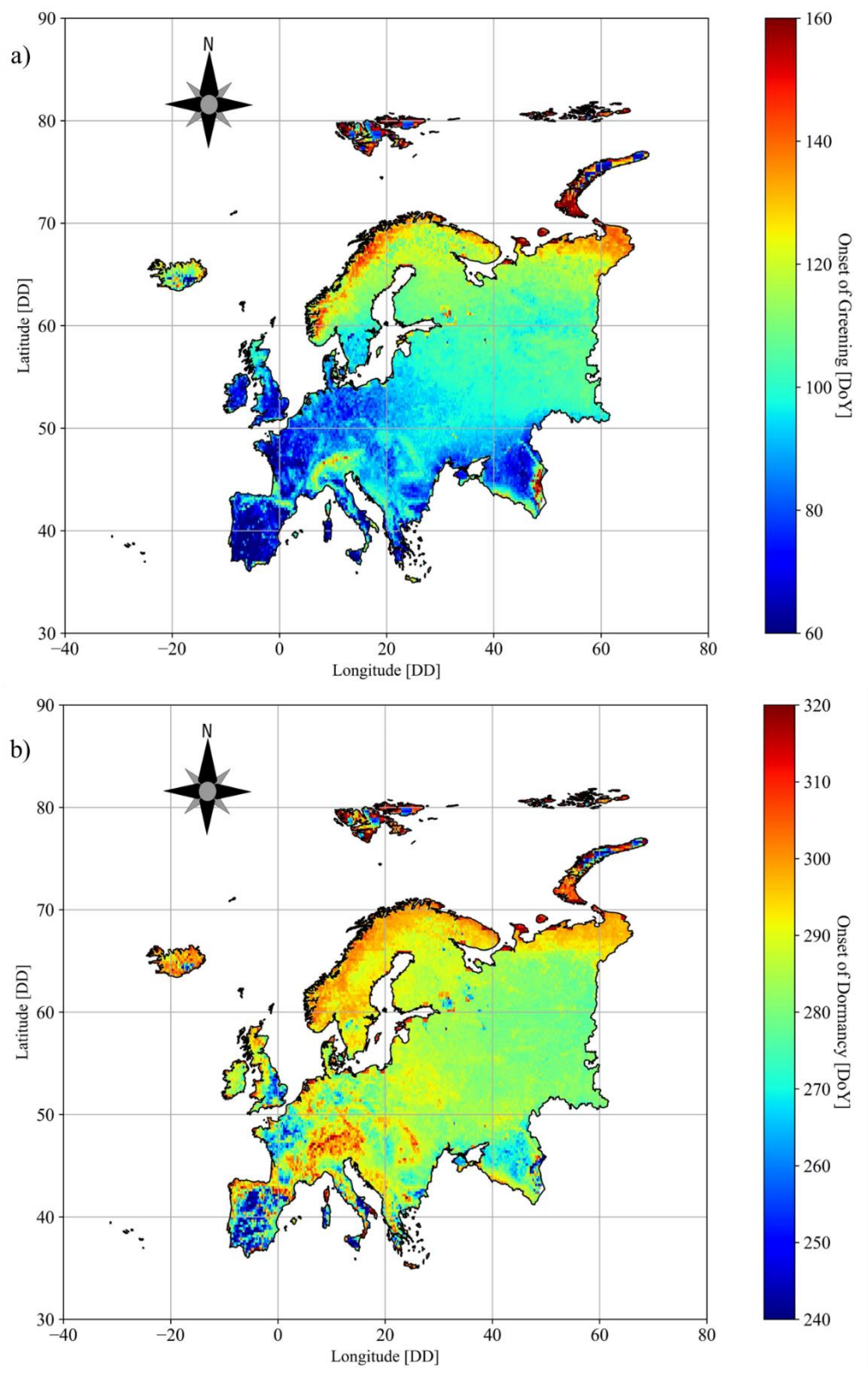

Supplementary Figure 1 | Variation of the long-term (1982-2020) average of onsets of greening (a) and dormancy (b) across Europe.

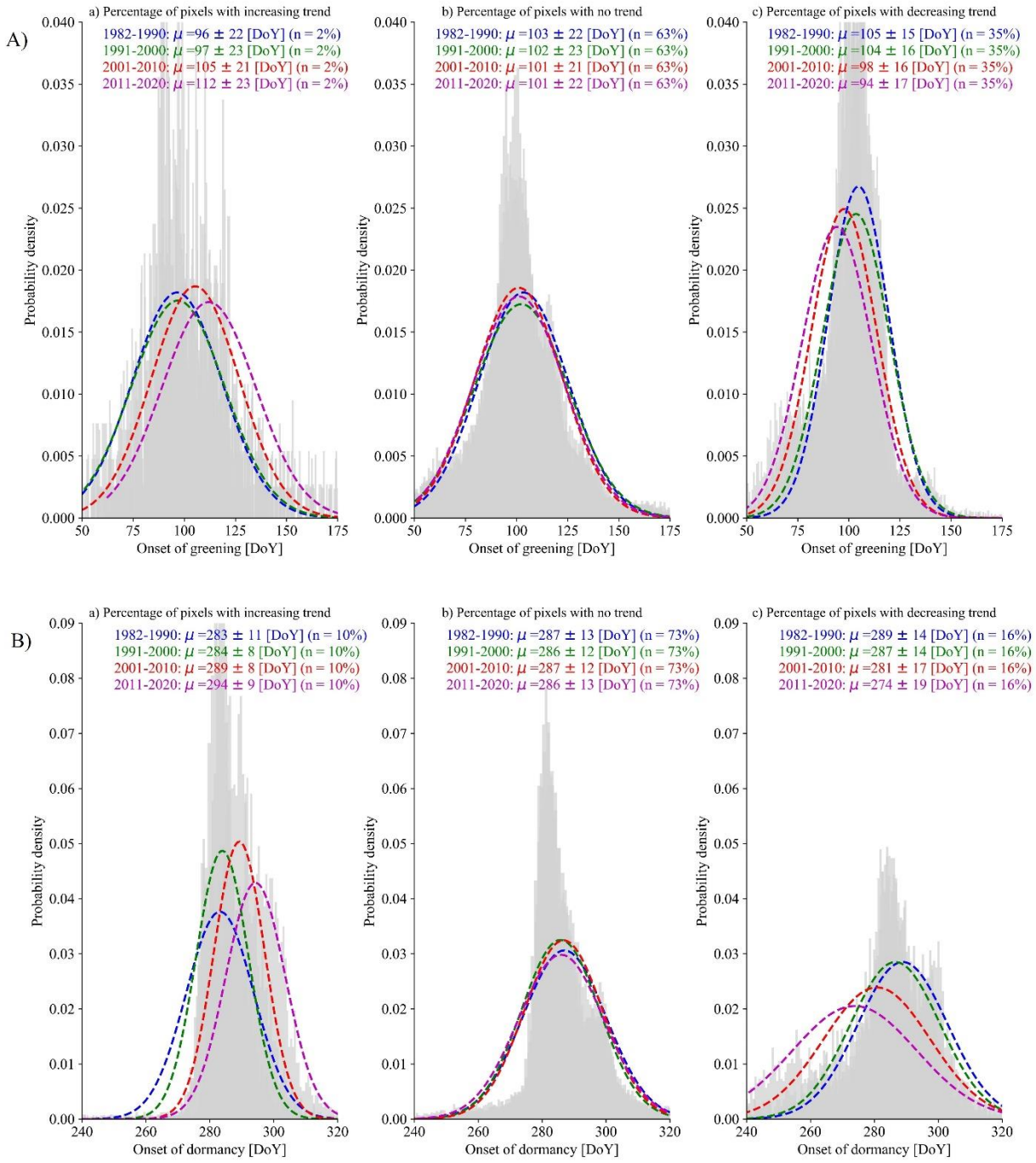

Supplementary Figure 2 | Histograms and probability distribution functions (PDFs, dashed lines) of the onsets of greening (A) and dormancy (B) in different decades. Panel (a) shows the histograms and PDFs for pixels with increasing trend, panel (b) for pixels with decreasing trend and panel (c) for pixels without significant trend. The letter μ corresponds to the mean ± standard deviations and n corresponds to the percentage of pixels in each group.

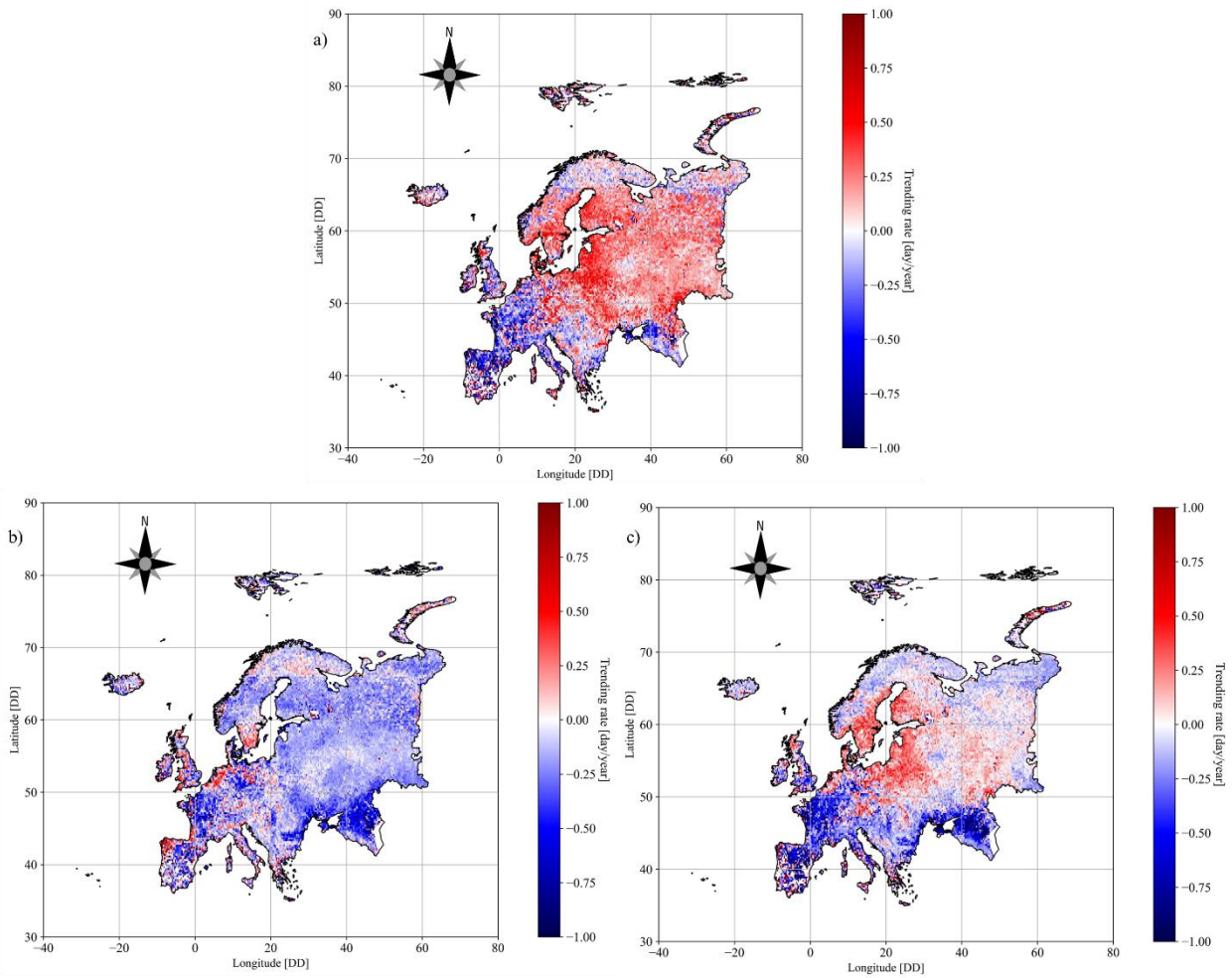

Supplementary Figure 3 | Variation of the long-term (1982-2020) trend of length of growing season (a), onset of greening (b), and onset of dormancy (c) in Europe. Positive and negative trending rates respectively mean lengthening and shortening of growing season or later and earlier onset of greening and dormancy. The analysis is based on the implementation of the original nonparametric test of Mann-Kendall[1,2] trend analysis testing the significance of change of data by time. The color bar is intentionally limited to +1 and -1 (obtained from the map histogram) to increase the contrast of the map.

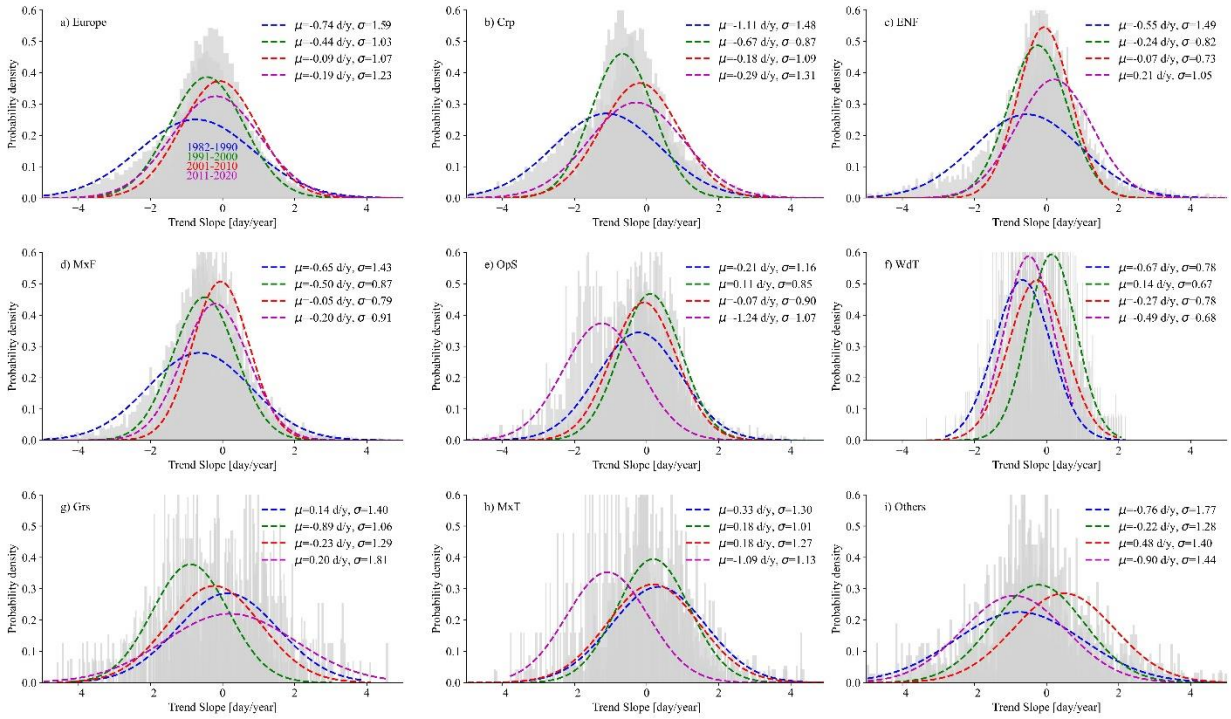

Supplementary Figure 4 | Histograms and probability distribution functions (PDFs) of trends in the slope of the onset of greening in different decades under different land cover types. The changes are quantified by trend parameter obtained from Mann-Kendall analysis. Panel (a) shows the histograms (grey bars) and PDFs (dashed lines) for entire Europe, panel (b) for croplands (Crp), panel (c) for evergreen needleleaf forests (ENF), panel (d) for mixed forest (MxF), panel (e) for open shrublands (OpS), panel (f) for wooden tundra (WdT), panel (g) for grasslands (Grs), and panel (i) for mixed tundra (MdT). The letter μ and σ correspond to the mean and standard deviations.

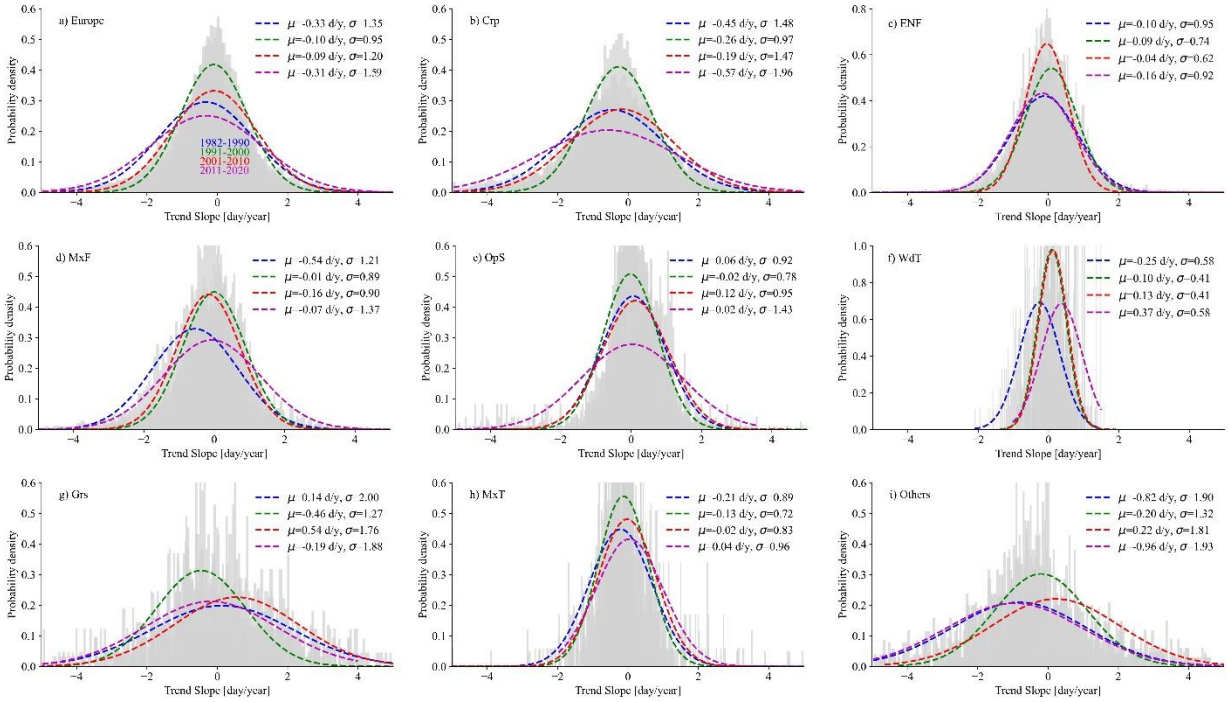

Supplementary Figure 5 | Histograms and probability distribution functions (PDFs) of trends in the slope of the onset of dormancy in different decades under different land cover types. The changes are quantified by trend parameter obtained from Mann-Kendall analysis. Panel (a) shows the histograms (grey bars) and PDFs (dashed lines) for entire Europe, panel (b) for croplands (Crp), panel (c) for evergreen needleleaf forests (ENF), panel (d) for mixed forest (MxF), panel (e) for open shrublands (OpS), panel (f) for wooden tundra (WdT), panel (g) for grasslands (Grs), and panel (i) for mixed tundra (MdT). The letter μ and σ correspond to the mean and standard deviations.

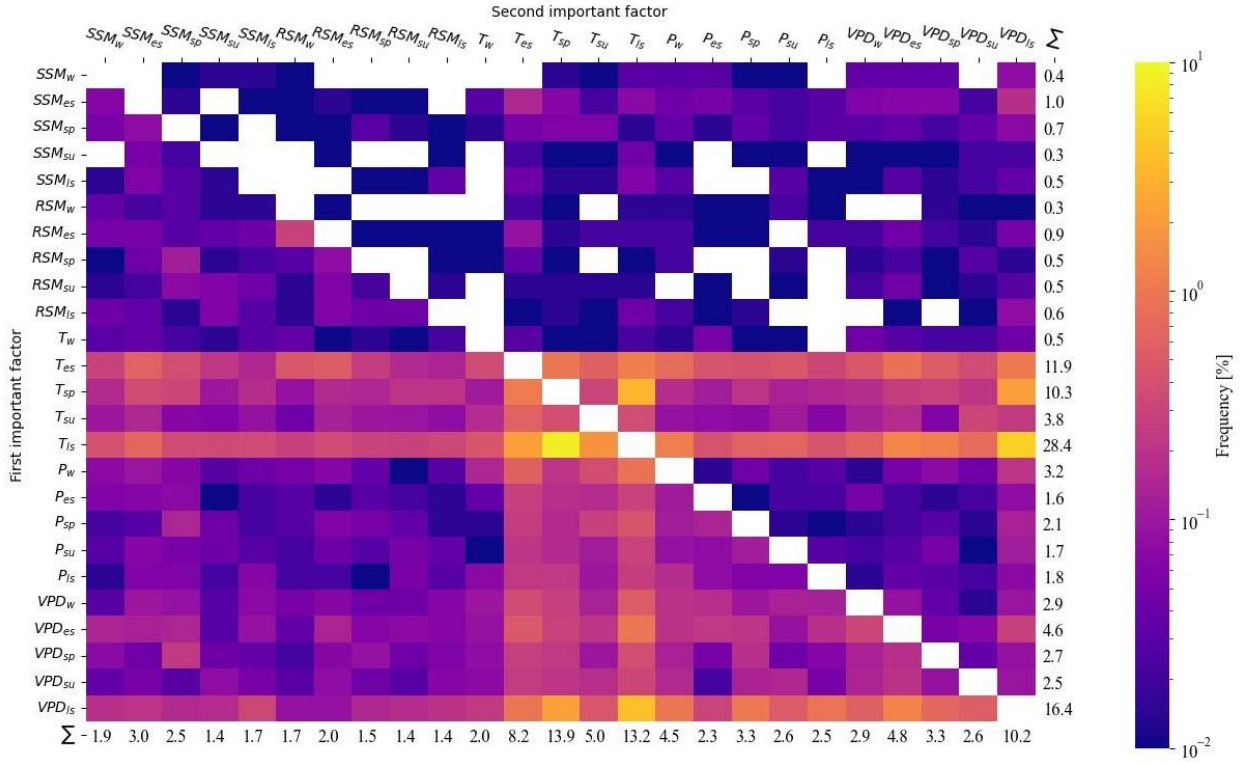

Supplementary Figure 6 | The first and second most important control factors of length of season across Europe. SSM and RSM refer to surface soil moisture and root zone soil moisture, respectively, T is temperature, P precipitation, and VPD vapor pressure deficit. Subscripts w, es, sp, su and ls refer to winter, early spring, spring, summer, and late summer periods.

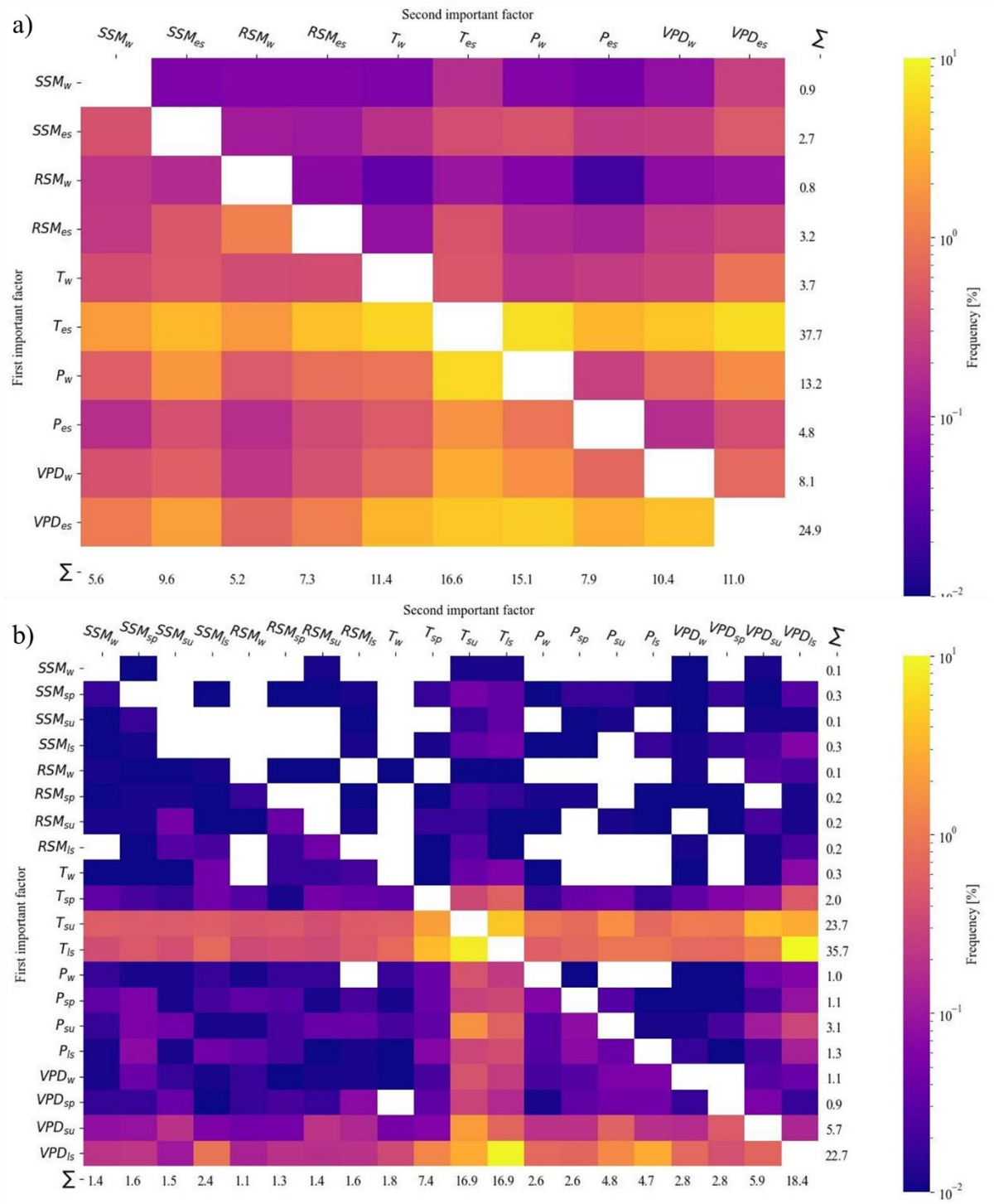

Supplementary Figure 7 | The first and second most important control factors of onsets of greening (a) and dormancy (b) across Europe. SSM and RSM imply soil moisture at surface and rooting depth, respectively, T implies temperature, P implies precipitation, and VPD implies vapor pressure deficit. Subscripts w, es, sp, su, and ls imply winter, early spring, spring, summer, and late summer periods.

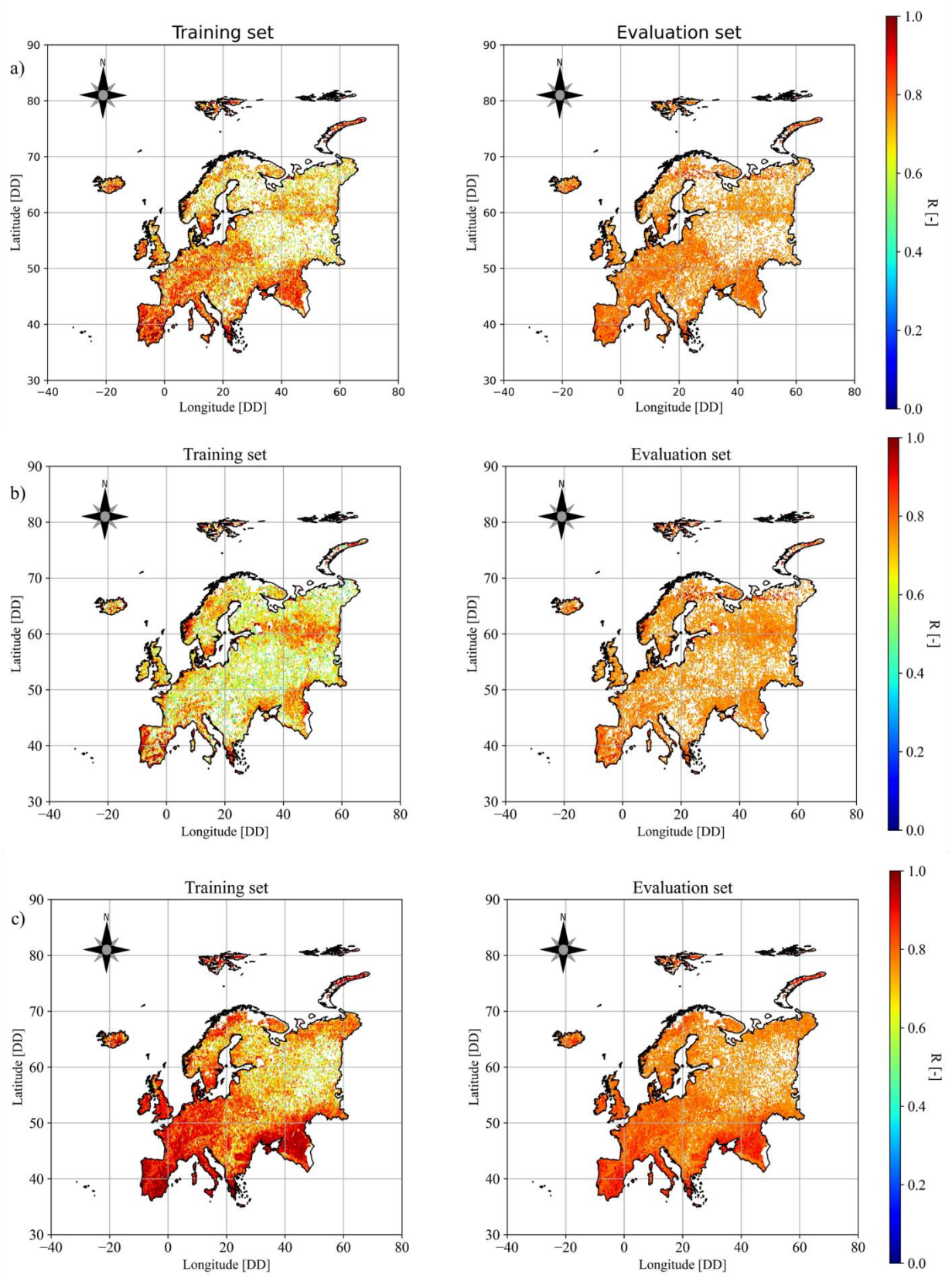
a)
Training set
Evaluation set
b)
Training set
Evaluation set
c)
Training set
Evaluation set
N
Latitude [DD]
Longitude [DD]
R [-]
90
80
70
60
50
40
30
−40
−20
0
20
40
60
80
1.0
0.8
0.6
0.4
0.2
0.0

Supplementary Figure 8 | The mean accuracy of the fitted model to predict length of growing season (a), onset of greening (b), and onset of dormancy (c) using main meteorological data plus soil water content at surface soil and rooting depth. The R corresponds to the Pearson correlation between the calculated season length and that predicted by the model. Training and evaluation sets refer to subsets of data that are used to train and evaluate the developed networks by randomly splitting the data into them, with 70 percent of the data used to train the networks and the rest used to test them as independent data.

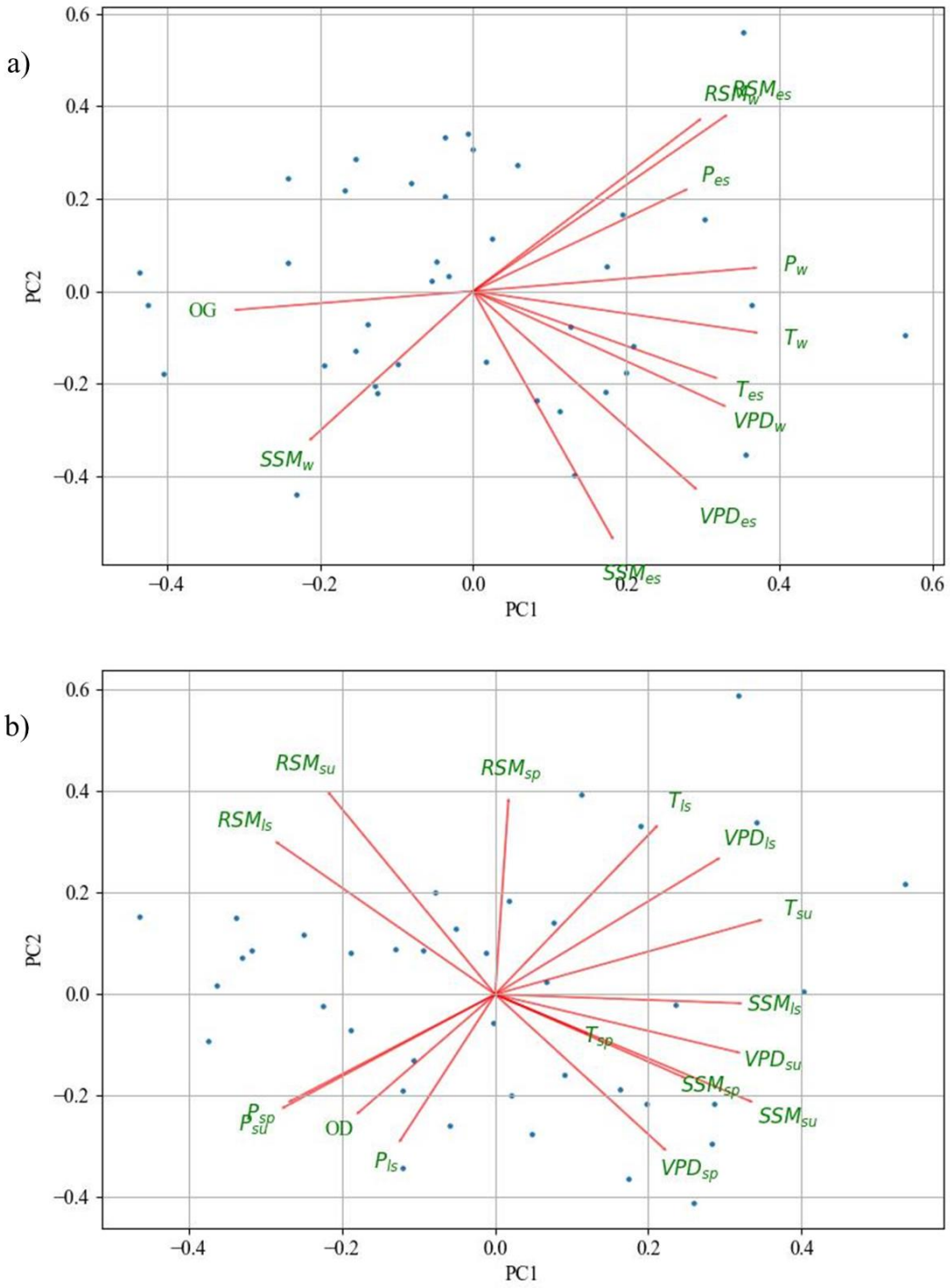

Supplementary Figure 9 | Relationship between onset of greening (a) and onset of dormancy (b) and meteorological and soil variables. OG and OD refer to onsets of greening and dormancy, SSM and RSM refer to surface soil moisture and root zone soil moisture, T is temperature, P precipitation, and VPD vapor pressure deficit. Subscripts w and es refer to winter and early spring periods which parameters are averaged for.

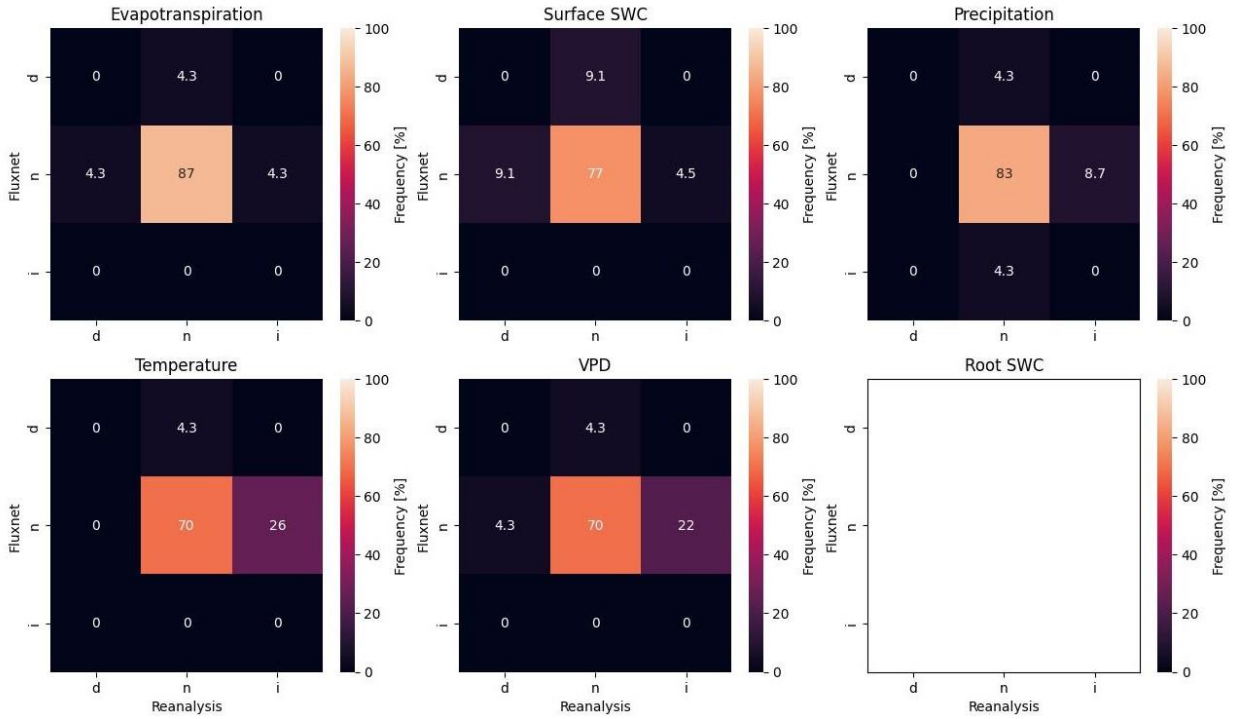

Supplementary Figure 10 | Heatmaps showing the confusion matrix between existing trends from FLUXNET and reanalysis data on evapotranspiration, soil water content (SWC) at the soil surface, precipitation, temperature, and vapor pressure deficit (VPD). No SWC was reported in the root zone in the FLUXNET database. A total of 25 FLUXNET stations with data from 2000 to 2017 were included in this analysis. In heatmaps, the x-axis corresponds to the reanalysis data and the y-axis corresponds to the FLUXNET data. The x and y labels of i, n and d correspond to an increasing trend, no trend, and a decreasing trend in the Mann-Kendall analysis.

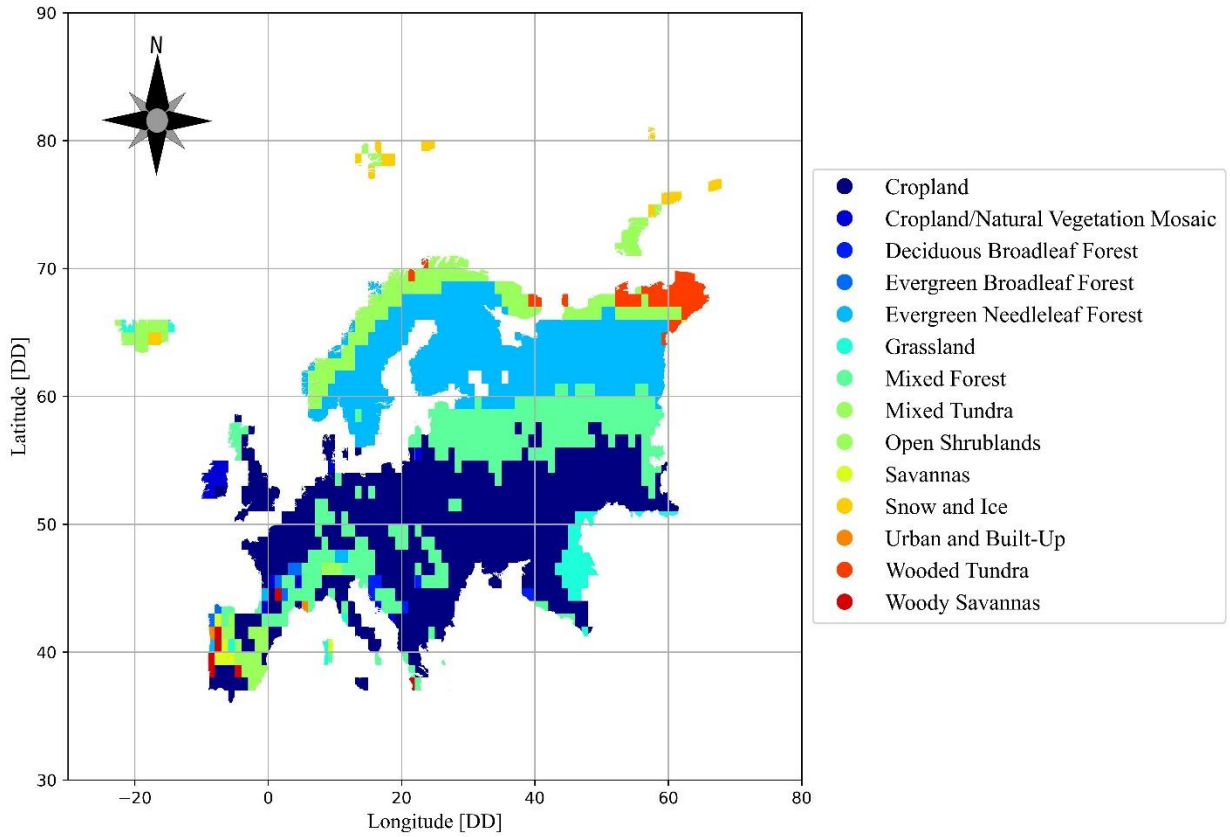

Supplementary Figure 11 | GLDAS Vegetation Class/Mask used in this investigation.

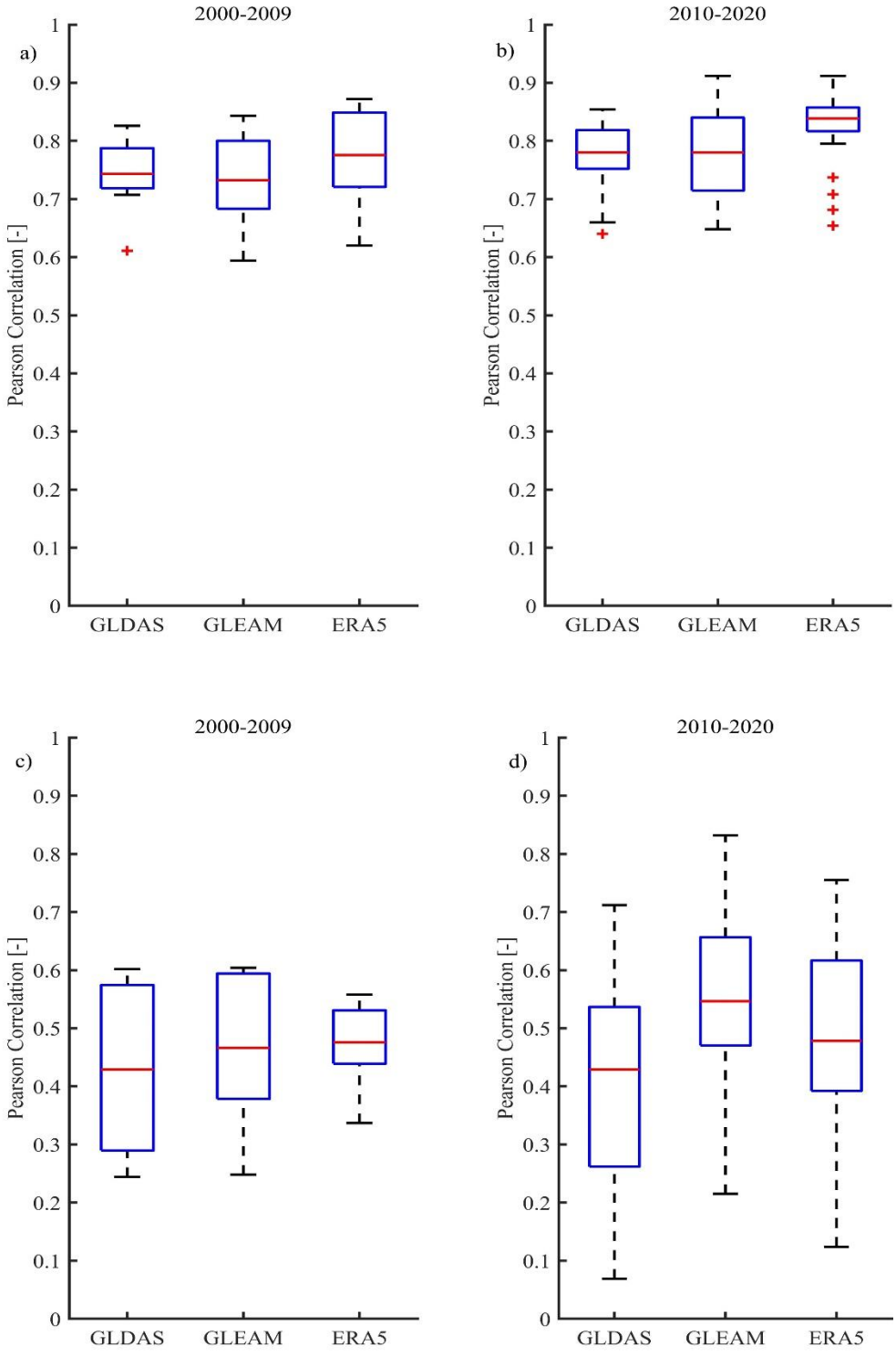

Supplementary Figure 12 | Pearson correlations between FLUXNET evapotranspiration, ET, (a and b) and surface soil moisture, SSM, (c and d) data and ET and SSM of other datasets (GLDAS, GLEAM, and ERA5-land).

Supplementary Table 1 | Variation different variables averaged over summer [peaking time of greening till onset of dormancy] in different decades and areas with significant decreasing, increasing, or no trend obtained from Mann-Kendal analysis. The reported values correspond to the mean ± standard deviations.

Trend type	Period	ET [mm/d]	SSM [cm^3/cm^3]	RSM [mm]	P [mm/d]	T [C]	VPD [kPa]
Increasing	1982-1990	1.39 ± 0.76	0.28 ± 0.06	371.51 ± 176.90	1.02 ± 0.38	10.89 ± 4.32	0.31 ± 0.20
	1991-2000	1.49 ± 0.85	0.30 ± 0.05	376.75 ± 172.50	1.36 ± 0.47	11.43 ± 4.28	0.37 ± 0.22
	2001-2010	1.66 ± 0.86	0.31 ± 0.05	393.27 ± 169.59	1.71 ± 0.55	12.40 ± 4.07	0.41 ± 0.25
	2011-2020	1.80 ± 0.90	0.32 ± 0.06	394.76 ± 170.85	1.60 ± 0.40	12.96 ± 4.26	0.43 ± 0.28
No trend	1982-1990	1.51 ± 0.64	0.28 ± 0.41	385.63 ± 169.42	1.99 ± 0.91	11.38 ± 3.31	0.29 ± 0.19
	1991-2000	1.56 ± 0.72	0.28 ± 0.41	368.82 ± 165.09	2.16 ± 0.87	11.68 ± 3.43	0.34 ± 0.21
	2001-2010	1.58 ± 0.66	0.29 ± 0.41	369.48 ± 159.94	2.19 ± 0.82	11.97 ± 3.28	0.34 ± 0.21
	2011-2020	1.57 ± 0.69	0.29 ± 0.41	367.20 ± 166.05	1.74 ± 0.71	11.88 ± 3.36	0.34 ± 0.22
Decreasing	1982-1990	1.50 ± 0.57	0.24 ± 0.05	386.72 ± 151.45	2.26 ± 0.68	12.14 ± 2.25	0.29 ± 0.21
	1991-2000	1.48 ± 0.59	0.23 ± 0.06	366.87 ± 151.16	2.03 ± 0.59	12.38 ± 2.27	0.31 ± 0.21
	2001-2010	1.36 ± 0.57	0.22 ± 0.06	352.44 ± 152.70	1.99 ± 0.58	11.50 ± 2.16	0.26 ± 0.19
	2011-2020	1.20 ± 0.54	0.21 ± 0.06	342.82 ± 157.53	1.54 ± 0.46	10.65 ± 2.16	0.23 ± 0.17
	Frequencies [%]						
Increasing	-	30.9	20.2	1.5	0.5	46.5	34.9
No trend	-	65.3	74.6	89.2	59.7	52.6	64.6
Decreasing	-	3.9	5.2	9.3	39.8	0.9	0.5

ET stands for evapotranspiration, SSM for soil moisture at the surface, RSM for soil moisture in the root zone, P for precipitation, T for temperature, and VPD for vapor pressure deficit.

Supplementary Note

Phenological stages of different vegetation types

In inferences from remote sensing, researchers, e.g., Zhang, et al. [3], typically characterize the annual cycle of vegetation phenology by four key transition dates: Greening, Maturation, Senescence, and Vegetation Dormancy. These dates define the major phenological phases of vegetation dynamics on annual time scales. As outlined by Zhang, et al. [3], greening is the date when photosynthetic activity begins; maturity refers to the date when the plant's green leaf area is greatest; senescence means the date when photosynthetic activity and green leaf area begin to decline rapidly; and finally, dormancy refers to the date when physiological activity approaches zero. This is true for almost all vegetation types, with only some differences in evergreen needleleaf forests. In evergreen forests dominated by conifers that retain their needles throughout the year, phenological phases are generally less pronounced than in deciduous forests[4] as well as other vegetation types. Evergreen trees do not lose their leaves all at once like deciduous trees[5], so there is no clearly delineated period of leaf senescence and dormancy. Nevertheless, there are some recognizable phenological phases in evergreen forests, such as budburst [when new growth emerges from buds, as in greening of other vegetation types], active growth [which occurs throughout the year if environmental conditions such as temperature and humidity are favorable, so that trees produce new needles and cones and continue to grow in height and width], and dormancy. Although evergreen trees do not lose their leaves all at once, they may enter a dormant period during the winter months when growth slows due to colder temperatures and less sunlight[6]. Autumn dormancy in evergreen forests is a deactivation of photosynthesis[6] rather than a loss of their leaves. Yin, et al. [7] note that phenological changes in evergreen forests generally occur at the photosynthetic level but can still be detected by structural and physiological vegetation indices. Our visual inspection of the NDVI curve for evergreen needleleaf forests also confirms that while the annual NDVI curve of evergreen needleleaf forests does not vary as much as other vegetation types, it still provides enough information to identify the beginning and end of the active growing season in these forests.

Supplementary Discussion 1

Use of NDVI data to characterize the phenological stages of vegetation types

The Normalized Difference Vegetation Index (NDVI) is a commonly used remote sensing index that measures the greenness and vegetation density of an area by analyzing the difference between

the red and near-infrared bands of the electromagnetic spectrum[8,9]. Seasonal changes in NDVI can provide valuable information on vegetation dynamics and productivity in different vegetation types[10]. Pinzon and Tucker [10] have highlighted the importance of seasonal changes in NDVI for monitoring vegetation dynamics and productivity in various types of ecosystems. Here is some information on what seasonal NDVI changes can provide in different vegetation types[11-13]:

Grasslands and Savannas:

In grasslands and savannas, NDVI values are typically highest during the wet season when there is an abundance of moisture and vegetation growth is most active. During the dry season, NDVI values typically decrease as vegetation becomes less dense and some plants become dormant or die off. Seasonal NDVI changes in grasslands and savannas can provide information on the timing and duration of the growing season, as well as the effects of drought and other environmental factors on vegetation productivity.

Forests:

In forests, NDVI values can vary depending on the type of vegetation present. Broadleaf forests typically have higher NDVI values during the growing season when leaves are present, and lower NDVI values during the winter months when leaves have fallen. On the other hand, evergreen needleleaf forests, also known as coniferous forests, typically experience less seasonal variation in their vegetation compared to deciduous forests since their foliage is present year-round. In evergreen needleleaf forests, NDVI values tend to remain relatively stable throughout the year, with a slight increase in the growing season during spring and summer, followed by a slight decrease in the fall and winter. In total, the magnitude of this seasonal variation is generally smaller than that observed in deciduous forests. However, Liu, et al. [14] showed that although canopy NDVI had a small dynamic range for evergreen species, they were still able to distinguish a clear pattern for NDVI enabling them to characterize the start and end of the season in evergreen forests. In general, seasonal NDVI changes in forests can provide information on the timing and duration of the growing season, as well as the effects of disturbances such as fires or logging.

Croplands:

In croplands, NDVI values are typically highest during the growing season when crops are actively growing, and vegetation density is at its highest. NDVI values may decrease during the off-season or fallow periods and after harvest when crops are not present. Seasonal NDVI changes in

croplands can provide information on growing season length, crop yield, crop health, and the effects of environmental factors such as drought or pest infestations.

Wetlands:

In wetlands, NDVI values can vary depending on the type of vegetation present. Emergent vegetation such as cattails or reeds typically have high NDVI values during the growing season when vegetation density is highest. In contrast, submerged vegetation such as algae or seagrasses may show less seasonal variation in NDVI values. Seasonal NDVI changes in wetlands can provide information on the timing and duration of the growing season, as well as the effects of disturbances such as flooding or changes in water levels.

Overall, seasonal NDVI changes can provide valuable information on vegetation dynamics and productivity in different vegetation types, helping to monitor the health and resilience of ecosystems and inform land management decisions. For more information on advantages and challenges in monitoring vegetation phenology stages from space, one may refer to the review paper conducted by Ma, et al. [15].

Supplementary Discussion 2

Additional analysis to determine control factors for temporal change in OG and OD

To test whether the hypothesis that SM is not a control factor for the timing of OG and OD, but VPD is a control factor, is correct, we performed an additional evaluation on the temporal evolution of ET, RSM, SSM, T, VPD, and P data averaged for summertime [from the peaking time of greening till onset of dormancy]. We first analyzed the general trend of the above variables for the entire period (1982-2020) and then calculated the decade-wise mean value of these variables for different areas with increasing, decreasing and no trend (the results are reported in the supplementary Table in above). 89% of the pixels in Europe show no significant trend for the summer RSM where the mean value of different decades for these areas varies around 367 to 386 mm. Similarly, 75% of the pixels show no significant trend for the summer SSM, and 20% show an increasing trend. 60% of the pixels also show no significant trend for summer P, but 40% show a decreasing trend where daily averaged summertime rainfall is decreased from 2.26 to 1.54 mm/d. 47% of the pixels show a significant increase of 2.0°C for summer T in the last decade (2011-2020) compared to the first decade (1982-1990). For the remaining 53% of pixels, we still record a 0.5°C increase in summer T, although the trend is not significant. 35% of the pixels show a

significant increase for summer VPD, with 120 Pa higher VPD in the last decade (2011-2020) than in the first decade (1982-1990). The remaining pixels show an increase of 50 Pa in the last decade compared to the first decade, even though the trend is not significant. Interestingly, for 65% of the pixels there is no significant trend for summer ET (showing a mean value of 1.51 to 1.58 mm/d) and only for 31% of pixels we see and increasing trend where ET is increased from 1.40 mm/d in first decade to 1.80 mm/d in the last decade. For the remaining pixels we see no significant change in ET values among different decades. This means that some factor other than water availability is controlling summer ET otherwise we would see an increase in ET accompanied by depletion in the SSM and RSM. However, as reported by Graf, et al. [16], it can be argued that no change in ET can be the net result of a simultaneous increase in potential ET along with a decrease in the availability of water for evapotranspiration. However, we already show that there is no such decrease in water availability during the summer in our case. This confirms our hypothesis that although there is still sufficient water for ET and promising atmospheric conditions for soil water transpiration, AWD exceeds the water supply rate of plants and then wilt/senescence sets in. For cropland, the story might be different. The higher T-value probably leads to an earlier harvest on arable land, and after that there is usually no new crop or no plants with a high LAI on the land.

To confirm the obtained trend for the above-mentioned variables using in situ data, we performed a Mann-Kendall trend analysis over those variables obtained from the FLUXNET database and compared them to obtained results for the corresponding pixels in the reanalysis data using an error matrix (see supplementary Fig. 10 above). A total of 25 FLUXNET stations in Europe contain (almost) complete data from 2000 to 2020. Overall, the trends obtained from both in situ and reanalysis data agree 87% for ET, 77% for SSM, 83% for P, 70% for T, and 70% for VPD. Therefore, we can be confident that our conclusion can also be confirmed by ground observation data.

Supplementary References:

1 Mann, H. B. Nonparametric tests against trend. *Econometrica: Journal of the econometric society*, 245-259 (1945).

2 Kendall, M. G. Rank correlation methods. (1948).

3 Zhang, X. *et al.* Monitoring vegetation phenology using MODIS. *Remote sensing of environment* **84**, 471-475 (2003).

4 Williams-Linera, G. Phenology of deciduous and broadleaved-evergreen tree species in a Mexican tropical lower montane forest. *Global Ecology and Biogeography Letters*, 115-127 (1997).

5 Kobayashi, H. *et al.* In Situ Observations Reveal How Spectral Reflectance Responds to Growing Season Phenology of an Open Evergreen Forest in Alaska. *Remote Sensing* **10**, 1071, doi:10.3390/rs10071071 (2018).

6 Richardson, A. D. *et al.* Terrestrial biosphere models need better representation of vegetation phenology: results from the North American Carbon Program Site Synthesis. *Global Change Biology* **18**, 566-584, doi:10.1111/j.1365-2486.2011.02562.x (2012).

7 Yin, G., Verger, A., Filella, I., Descals, A. & Peñuelas, J. Divergent estimates of forest photosynthetic phenology using structural and physiological vegetation indices. *Geophysical Research Letters* **47**, e2020GL089167 (2020).

8 Tucker, C. J. Red and photographic infrared linear combinations for monitoring vegetation. *Remote sensing of Environment* **8**, 127-150 (1979).

9 Vilhar, U. *et al.* in *Developments in Environmental Science* Vol. 12 (eds Marco Ferretti & Richard Fischer) 169-182 (Elsevier, 2013).

10 Pinzon, J. E. & Tucker, C. J. A Non-Stationary 1981–2012 AVHRR NDVI3g Time Series. *Remote Sensing* **6**, 6929-6960 (2014).

11 Miao, L., Müller, D., Cui, X. & Ma, M. Changes in vegetation phenology on the Mongolian Plateau and their climatic determinants. *PLOS ONE* **12**, e0190313, doi:10.1371/journal.pone.0190313 (2017).

12 Zheng, Y. *et al.* Vegetation response to climate conditions based on NDVI simulations using stepwise cluster analysis for the Three-River Headwaters region of China. *Ecological Indicators* **92**, 18-29, doi:https://doi.org/10.1016/j.ecolind.2017.06.040 (2018).

13 Lobell, D. B. & Asner, G. P. Cropland distributions from temporal unmixing of MODIS data. *Remote Sensing of Environment* **93**, 412-422 (2004).

14 Liu, Y. *et al.* Improved modeling of land surface phenology using MODIS land surface reflectance and temperature at evergreen needleleaf forests of central North America. *Remote Sensing of Environment* **176**, 152-162, doi:https://doi.org/10.1016/j.rse.2016.01.021 (2016).

15 Ma, X. *et al.* Monitoring nature's calendar from space: Emerging topics in land surface phenology and associated opportunities for science applications. *Global Change Biology* **28**, 7186-7204 (2022).

16 Graf, A. *et al.* Altered energy partitioning across terrestrial ecosystems in the European drought year 2018. *Philosophical Transactions of the Royal Society B: Biological Sciences* **375**, 20190524, doi:doi:10.1098/rstb.2019.0524 (2020).